

Facsimile: +44 1235 466435
Telephone: +44 1235 464181

United Kingdom
OX14 3DB
Oxfordshire
Abingdon
Culham Science Centre

EURATOM/UKAEA Fusion Association

© UKAEA

August 2002

A. Thyagaraja, N. Loureiro and P.J. Knigght

Spectral and evolutionary analysis of
advection-diffusion equations and the shear
flow paradigm

EURATOM/UKAEA Fusion

UKAEA FUS 477

A. Thyagaraja, N.ourero^(a) and P.J. Kingley
EURATOM/UKAEA Fusion Association, Culham Science Centre, Abingdon, OX14
^(a) Plasma Physics Group, Imperial College of Science, Technology and Medicine,
London SW7 2AZ, UK.

Spectral and evolutionary analysis of
advection-diffusion equations and the shear flow
paradigm

Advection-diffusion equations occur in a wide variety of fields in many contexts of active and passive transport in fluids and plasmas. The effects of sheared advective flows in the presence of irreversible processes such as diffusion and viscosity are of considerable key role in both transport and the dynamical structures characteristic of electromagnetic turbulence. In this paper we investigate the spectral and evolutionary properties of plasma turbulence, the physically interesting limit of small (but finite) diffusion is studied in detail. In particular, the analytical work is extended and supplemented by numerical techniques involving a direct solution of the eigenvalue problem as well as evolutionary studies of the initial value problem using a parallel code, CADENCE. The three approaches are complementary and entirely consistent with each other when appropriate comparison is made. They reveal different aspects of the properties of the advection-diffusion equation, such as the ability of sheared flows to generate a direct cascade to high wave numbers transverse to the advection and the consequent enhancement of even small amounts of diffusivity. The inviscid, jet-like flows to "confine" transport to low shear regions are demonstrated. The implications of these properties in a wider context are discussed and set in perspective.

Abstract

We consider a simple two-dimensional problem. Let R be a two-dimensional domain defined by the rectangle, $0 \leq x \leq L_x, 0 \leq y \leq L_y$. We shall be interested in a scalar

II. Formulation of the model and analytic results

The paper is organized as follows: In Section II we discuss the mathematical formulation of the linear advection-diffusion model and analytical properties of the system. In Section III, the numerical and analytical solutions to certain solvable cases of the system are presented and their properties discussed. Section IV is devoted to the solution of the initial value problem and the evolutionary approach using the parallel processing code CADENCE which presents a typical example of the approaches taken in the computational physics of fully nonlinear plasma turbulence simulations. The paper concludes with some discussion of the results and the contexts in which the insights obtained lead to useful conclusions.

The purpose of the present paper is to understand and lay bare the essential features of the diffusion-advection-diffusion problems in more complicated (including nonlinear) physical situations [5]. In this connection, Refs. [7, 8] may also be consulted for additional examples of the utility of the spectral approach in understanding the properties of equations encountered in plasma and fluid theory. Furthermore, the advection-diffusion equation is used as the simplest, paradigmatic example to model a specific domain evolution of advection-diffusion problems in more complicated (including nonlinear) situations [5]. It will be shown that even this simplified model possesses a number of unexpected and remarkable spectral properties which throw light on the self adjoint, dissipative system. It will be shown that this simplified transport is a non-linear, but turns out to be far from trivial, as one still has to deal with a non-self adjoint, dissipative system. The equation for passive transport is also assumed to be known. The equation for passive transport is shear so that the model used captures the key features of more complicated systems. The diffusivity is also assumed to be known. The equation for passive transport is to its essentials by taking the flow to be given, and assigning specific properties such as density (or, the *turbulent fluctuations in such quantities*). The phenomenon is simplified of the interaction between flows and transport of some property, such as temperature or density via the so-called "zonal" $E \times B$ flows (see Refs. [1-6]) have been identified as important elements in the formation of internal and edge transport barriers. Transport barriers are regions of high gradients of density and/or temperature which form spontaneous and regular to be closely associated with zonal flows. These are $E \times B$ flows transverse which appear to be associated with zonal flows. The phenomenon is found in fusion plasmas on the other, to exert a stabilizing influence on the turbulence.

The simplest of all transport equations is the advection-diffusion equation characterizing "passive scalar" transport by a specified velocity field. This type of equation has been analyzed over many years by many authors. It continues to form a key core of fluid and plasma transport theory. Perhaps, somewhat surprisingly, there remain important features of such equations which have yet to be fully elucidated. The most recent features of advection-diffusion phenomena are those encountered in fusion plasmas where the so-called "zonal" $E \times B$ flows (see Refs. [1-6]) have been identified as important elements in the formation of internal and edge transport barriers. Transport barriers are regions of high gradients of density and/or temperature which form spontaneous and regular to be closely associated with zonal flows. These are $E \times B$ flows transverse which appear to be associated with zonal flows. The phenomenon is found in fusion plasmas on the other, to exert a stabilizing influence on the turbulence.

I. Introduction

$$(5) \quad f(x, y, t) = \int_0^y F^0(x, y - u^y(t)) = \sum_{m=-\infty}^{\infty} f^m(x, 0) \exp[i k_y(y - u^y(t))]$$

solution for the equation is then given by
where $k_y \equiv 2\pi m/L_y$, and $m = 0, \pm 1, \pm 2, \dots$. Now suppose that $v \equiv 0$. The explicit

$$(4) \quad \frac{\partial}{\partial f^m} = -ik_y u^y(x) f^m - ik_y^2 f^m + v \frac{\partial^2 f^m}{\partial x^2}$$

Substituting in Eq.(1), we find that the amplitudes satisfy the infinite set of equations,

$$(3) \quad f(x, y, t) = \sum_{m=-\infty}^{\infty} f^m(x, t) \exp(i 2\pi m y/L_y)$$

We now demonstrate the direct cascade property alluded to above. Since f is periodic in y , we develop the solution in a Fourier series:

All the effects considered occur even when only diffusion in the x -direction, transverse to direction. d) For many purposes, it is not necessary to consider diffusion in the y -direction. develops, on a time-scale to be determined shortly, extreme fine-structure in the radial other words, the function $f(x, y, t)$ evolving according to the diffusionless equation quickly one obtains a very strong "direct cascade" of energy in k_x , the radial wave number. In that although there are an infinity of conserved constants, and is fully time-reversible, c). If the diffusivity, $v = 0$, the equation can be solved exactly and the solution reveals the advection, is retained.

$$(2) \quad \frac{d}{dt} \left(\int_{L_y}^0 \int_{L_x}^0 f^2 dy dx \right) = -v \int_{L_y}^0 \int_{L_x}^0 \left[\frac{\partial f}{\partial y} \left(\frac{\partial f}{\partial x} \right)^2 + \left(\frac{\partial f}{\partial x} \right)^2 \right] dy dx$$

obtained by integration by parts:
is always stable, irrespective of u^y . This follows from the "H-theorem" which is readily have a unique solution for "resonable" initial data on f and suitable u^y . b) The system Equation (1) is linear, and the initial-boundary problem thus posed is easily shown to We begin the analysis by noting some elementary facts pertaining to our model. a)

sytem.
therfore consists of elucidating the interplay of the advection and diffusion in this simple direction, but *diffused* in the radial and poloidal directions. Our fundamental problem magnetic flux, density or any other physical quantity of interest) is *advection* in the poloidal states that under the influence of $u^y(x)$, the function f (this may represent temperature, where the advecting velocity, $u^y(x)$ is assumed to be a given function of x . The equation

$$(1) \quad \frac{\partial f}{\partial t} + u^y(x) \frac{\partial f}{\partial x} = v \left[\frac{\partial^2 f}{\partial x^2} + \frac{\partial^2 f}{\partial y^2} \right]$$

model we start with is represented by the advection-diffusion equation.
It is noted however that these are merely labels introduced to aid intuition. The basic tokamak physics and refer to the x -direction as "radial" and the y -direction as "poloidal". Suppose that v is a uniform and constant diffusivity. It is useful to make contact with satisfies (for simplicity) homogeneous boundary conditions at $x = 0, x = L_x$. We also function, $f(x, y, t)$ which is supposed to be periodic in y/L_y , with period 2π , and which

A second interesting feature revealed by Eq.(5) is the following: it is clear that the Fourier transform of f with respect to t gives a continuous spectrum in frequency (see also [7] for other examples). Thus, for each mode number m , the frequency of the mode, ω , varies

(subrange) whilst the dissipation takes place at around the cut-off at high k_x . The system typically at low to medium wave numbers (constituting the so-called inertial sheared advective transport characterizing the large-scale motions. The energy is fed into diffusion constitutes, in the limit of high Peclét numbers, a singular perturbation on the diffusion of v . This type of asymptotic behaviour is typical in both fluids and plasmas. Thus $\approx v_{-1/2}$. The dissipation rate becomes asymptotically (i.e., as $Pe \rightarrow \infty$) independent of k_x and higher values. The cut off values of k_x denoted by, k_{\max} are obviously at higher and lower values. The cascade in k_x tends to be cut off to zero, this term does not go to zero! Rather, the cascade in the system. The negative content of Eq.(2), which in fact describes the energy decay of the system. The negative of the RHS can be taken as the rate of entropy production in the system cuts off the direct cascade to entropy/heat production. This last statement is the diffusion cuts totally dominated by diffusion. We say that at high Peclét numbers the high k_x behaviour is as a function of x , for large times, it is never negligible, since the high k_x behaviour is (when the energy resides in the low k_x part of the spectrum and f is relatively smooth) occurs when $Pe = \infty$. If Pe is large, even if the diffusion term is initially negligible

Thus, a "small" corresponds to very large values of Pe . The situation described above

velocity itself.

number defined above contains the vorticity (or shearing rate) rather than the advection effects other than a trivial, real frequency change. For this reason, the Peclét always be removed by a Galilean transformation, and cannot therefore be responsible for the advection that is responsible for the effect in question, since any unshaded flow can interfereably. It is useful to note that it is the vorticity (equivalently, radial shear) in transport of momentum. In the following we shall use both Peclét and Reynolds numbers transport of momentum, which occurs naturally in problems involving advective-viscous known Reynolds number, which occurs naturally in problems involving advective-viscous relative importance of sheared advection to diffusion is exactly analogous to the well-known dimensional measure of the relative importance of the advection to diffusion is fundamental difference to that in which v is extremely small but finite. The appropriate In these circumstances, we can see immediately that the situation with $v \equiv 0$ will be

"vortices" or "corrugations" in the radial direction, transverse to the advection flow. Initially smooth (in x) function which varies in y , develops at later times, highly oscillatory from low k_x is transferred to high mode numbers, convectively. In physical space, an (i.e., shorter radial wave lengths). This is a form of "direct" cascade, whereby energy advection has the property of transporting energy in wave number space to higher k_x velocity u_y is nonunifrom (i.e., sheared in x). This immediately indicates that sheared by, $H = \int \int \left[\left(\frac{\partial f}{\partial t} \right)^2 + \left(\frac{\partial f}{\partial x} \right)^2 \right] dx dy$ grows unboundedly in time, so long as the advection is constant of the motion in this diffusionless system, the "entropy", defined indeed a solution that, provided $\frac{dx}{dt} \neq 0$, the radial derivative, $\frac{\partial f}{\partial x}$ grows unboundedly in time. This indicates that although the total "energy" defined by $E(t) = \int \int f^2 dx dy$, is solution from this, it is not hard to see from this

We next consider the second, more "natural" type of resolution of the continuum by real diffusion, which is an irreversible, entropy producing process. Thus relating the original

space, non-decaying "discreteum".

considerations similar to the ones above, to resolve the Alfvén continuum into a closely effect leading to tearing, within a two-fluid context. Such an effect would be expected, by law is *not* resistivity but electron inertia, which provides a purely non-dissipative, reactive is a paradigm for "collisionsless tearing", which occurs when the non-ideal effect in Ohm's although at first sight this looks far removed from classical physics, in actual fact, this preserving effect occurs as a singular perturbation on the advection of a complex scalar. can serve as a paradigm for a time-reversible system in which a purely *reactive*, entropy it is a complex quantity. The advection-diffusion equation with imaginary diffusivity the imaginary diffusion term. Of course, in this case, the meaning of ϕ is not clear as Thus, the continuum of the pure advection problem is "resolved" into a discreteum by real, nonzero number), all the eigenvalues ω must be real and form a discrete spectrum. An immediate consequence is that, irrespective of the size or sign of ω (so long as it is a

$$\frac{d^2\phi}{dx^2} = [u k_y^2 + k_y u_y(x) - \omega] \quad (7)$$

to the Sturm-Liouville problem in x with homogeneous boundary conditions: Equation (4) leads (upon introducing the harmonic time dependence, $k_m = \phi \exp(-i\omega t)$) be purely imaginary! Thus we set, $\omega = i\mu$, u is a real number with dimensions of diffusivity. First, let us consider an apparently "artificial" problem where the diffusivity ω is taken to

In the light of the fact that the diffusion term is a singular perturbation on the advection operator, the question naturally arises as to how the spectrum behaves when the Peclet number is large, but finite. It turns out that there are two distinct and rather different resolutions of this question depending on the detailed physics.

It is also evident that although ω itself does not "decay", just as in the Van Kampen Case theory of Landau damping, any integral over ω with respect to x would be transverse advection. Indeed, this simple advection diffusion model encapsulates all forms of continuum damping, be it in the theory of Alfvén waves, kinetic theory or radiative damping by a continuum of Van Kampen modes, as originally pointed out by Van Kampen himself [9].

$$\phi_m(\omega) = \frac{(\omega - u_y(x)k_y)}{\int u_y(x)k_y - \omega \phi_m(x) = 1} \quad (8)$$

obtained exactly as in the well-known Van Kampen-Case analysis from Eq.(4):

Furthermore, the "eigenfunction" corresponding to such a continuum eigenvalue is a singular (i.e., non normalizable), generalized function. These singular eigenfunctions are with the radial location x according to the "local" dispersion relation, $\omega(x) = u_y(x)k_y$.

$$F(x, p) = \int_{L_x}^0 T(x, x', p) h(x') dx' \quad (11)$$

Here $h(x)$ is the specified "initial" amplitude. This equation is to be solved for F , subject to (say) homogeneous boundary conditions at $x = 0, L_x$, where p is treated as an arbitrary complex parameter. From the preceding analysis, it is easily established that F is an analytic function of the complex variable p and has no singularities in the finite right half- p -plane. It is well-known that the solution of Eq.(10) may be represented in the form,

$$pF - h(x) = -ik_y u_y(x) F - ik_y^2 F + \frac{d^2 F}{dx'^2} \quad (10)$$

The transform function F then satisfies the inhomogeneous ordinary differential equation:

$$F(x, p) = \int_{\infty}^0 f \exp(-pt) dt \quad (6)$$

Henceforth, we simply suppress the suffix m , although this appears as a parameter in the m -modes. We take the Laplace transform of f with respect to t :

the m -modes. We take the Laplace transform of f with respect to t :

attempt to solve the initial-boundary value problem posed for this partial differential equation (PDE) in (x, t) for given m , by taking Laplace transforms. We note that the transformation between Laplace and Fourier transforms is well-known, and the use of the Laplace transform in initial-value problems follows Landau's approach to the Vlasov problem, and is merely one of convenience.

Let us return to the governing equation, Eq.(4) for the mode-amplitude, $f_m(x, t)$. We most general method applicable in principle to all nonself-adjoint problems. The Green's function method of Titchmarsh [10] which will now be described. It is the relevant eigenfunctions and eigenvalues. This "time-marching" approach is analogous to the initial value problem numerically and by suitable "filtering" procedures, extract the approach which will be the main focus of this paper. Finally, one could directly simulate the m -modes for arbitrary u, k_y for the given $u_y(x)$. It is this last and determine the eigenvalues for arbitrary u, k_y for the given $u_y(x)$. A complementary approach to this semi-analytic procedure would be to solve the equation numerically by Airy/Weber functions and the eigenvalues calculated numerically. A complementarity or quadrature functions, and the equation solved exactly in each approximation interval $u_y(x)$. Alternatively, to provide insight, $u_y(x)$ may be approximated by piecewise linear $u_y(x)$. Eq.(8) could be attacked by the complex WKB method for arbitrary but analytic is large) Eq.(8) must be square integrable in $0 \leq x \leq L_x$, as the potential has no singularities in this interval for any ω . When ω becomes small (ie., the Peclét number shows that the eigenvalues, ω must form a discrete spectrum, and furthermore, must lie in the lower half ω -plane. These facts are simple consequences of Eq.(2) and the observation that any solution of Eq.(8) must be square integrable in $0 \leq x \leq L_x$, as the potential has singularities in this case,

$$\frac{d^2 \phi}{dx'^2} = \frac{\omega}{[ik_y + i(k_y u_y(x) - \omega)]} \quad (8)$$

ω with the stipulation that it is real and positive, the eigenvalue problem for ϕ becomes

which require calculation of the eigenvalues by a suitable numerical method. We shall some specific profiles solutions can be found. These involve transcendental functions which has no general analytic solution for arbitrary velocity profiles, $V(x)$. However, for

$$\nu f''(x) + i(\lambda - m\nu V(x))f(x) = 0 \quad (14)$$

to solving the differential equation:

Let us set, without loss of generality, for convenience in what follows, $L_y = 2\pi$, $k_y = i\nu u_y(x) = V(x)$, $\lambda = \omega + \nu n^2$. The eigenvalue problem treated in this paper amounts

III. Analytical and Numerical Solutions of the Eigenvalue Problem

The above construction will be applied in simplified forms in the following to reveal the intricate and nontrivial spectra associated with the advection-diffusion equation. Instead of calculating the Green's function and locating its poles and residues in the left half-plane, we will directly solve the eigenvalue problem with $p = -i\omega$. Let us note that the method is also applicable, as it stands, when we include radial advection terms of the form, $\frac{\partial}{\partial x}(u_x(x)f)$, subject only to the proviso that there should not be any y -dependence in the radial advection component, u_x . If this requirement is not satisfied, variables do not separate and Fourier analysis in y does not help.

Pure imaginary do we obtain a classical, Hermitian, Sturm-Liouville operator. It is remarkable that this method works with essentially no change whether ν is real or complex (with positive real part). Note however that only in the special case when ν is real and can be written as a sum of contributions over the poles of L . As $t \rightarrow 0+$, we obtain the "spectral representation" or the eigenvalue expansion of the delta function. The half plane built into the Laplace transform. For $t > 0$, the contour is closed in the left half plane and may be taken along the imaginary p axis and closed by a semi-circular contour in the right half plane. The value is, of course zero, indicating consistency with the causality principle may be taken, for $t < 0$ along the imaginary p axis and closed by a semi-circular contour in

$$G(x, z, t) = \oint \frac{2\pi i}{dp} T(x, z, p) \exp(pt) \quad (13)$$

consequences. The Bromwich contour integral for real, positive ν , however small it may be. From this fact we deduce the following consequences. The Bromwich contour integral have poles in the left half (ie., $re(p) < 0$) p -plane; no other type of singularity is allowed with analytic coefficients and reasonably smooth functions $u_y(x)$ that $T(x, z, p)$ can only follows from standard theorems in the theory of second-order linear differential equations L , regarded as an analytic function of p , determine the behaviour in time of f . It readily yields a contour integral over the complex variable p , it follows that the singularities of T in this equation, $\delta(x - z)$ is Dirac's delta function. Since the inverse Laplace transform of

$$pT(x, z) - \delta(x - z) = -i\hbar_y u_y(x)T(x, z) - \nu k_y^2 T(x, z) + \nu \frac{\partial_x^2}{\partial^2 T}, \quad (12)$$

where the Green's function, $T(x, x, p)$ is also analytic in the complex variable p and satisfies,

$$\left(-\frac{1}{2} \sqrt{\frac{a}{i}} y^2 \right) f(x) \exp(u(x)) = f(x) u(x)$$

Simple algebraic reduction then leads to the Weber equation [11]. We now proceed in the usual way, by expressing the solution $f(x)$ in the form,

$$0 = f(xq + \frac{a}{i}) \frac{d}{dx} f - f \frac{d}{dx} \left(\frac{a}{i} \right) + \frac{d}{dx} \left(\frac{a}{i} \right) f^2 \quad (17)$$

where a and b are constants. The transverse advection diffusion equation then reduces to:

$$mV(x) = ux^2 + bq \quad (18)$$

We next consider a velocity profile of the type,

It is useful to observe that Airy functions can also be used whenever $V(x)$ is a piece-wise linear function of x . The solutions in different regions have to be "matched" at the points where the profile slope changes. The matching constants satisfy a linear homogeneous system, the determinant of which yields a transcendental equation for the eigenvalue, which requires a numerical solution technique (e.g. Newton-Raphson, or interval bisection). This model is useful for simulating irregular (but continuous) advection velocity profiles which are well-approximated by piece-wise linear functions.

It is useful to observe that Airy functions can also be used whenever $V(x)$ is a piece-wise linear function of x . The solutions in different regions have to be "matched" at the points where the profile slope changes. The matching constants satisfy a linear homogeneous system, the determinant of which yields a transcendental equation for the eigenvalue, which can be determined using the boundary conditions. Eigenvalues can then be obtained and determine the remaining constant using one of the boundary conditions. The other boundary condition then gives us an equation to which a root-finding method can be applied, hence determining the eigenvalues.

$$f(z) = C_1 Ai(z) + C_2 Bi(z) \quad (15)$$

The solutions of this are expressible in the form:

$$(z)fz = \frac{dz}{(z)f(z)}$$

reduces Eq.(14) to Airy's equation:

$$z = \frac{i(\alpha - m\zeta x)}{(\gamma - mn\zeta^2)}$$

We first consider the case of a linear velocity profile, $V(x) = Qx$ which has uniform shear/vorticity. This is the simplest case, the solution being given by a linear combination of Airy functions. Making the substitution

analyse three cases of the velocity profile $V(x)$ for which an analytic solution is possible: linear, parabolic and sinusoidal velocity profiles.

We briefly describe the numerical technique used to obtain discrete spectra. The shooting method is employed. This involves the specification of the values of the solution and its derivative at one of the boundaries (the left one, for instance), $f(0)$ and $f'(0)$ respectively, and a boundary condition at the right boundary, $f(L)$. Newton's method, applied to the solver of the initial-value problem and an initial guess for the eigenvalue λ , the solution can be calculated up to the right boundary, $f(L)$.

and A and B are integration constants. Eigenvalues can be calculated in the same semi-analytical way as described above, noting that the boundary conditions are now given by $f(\frac{L}{2}) = f(\frac{L}{2} - p\frac{\pi}{2}) = 0$.

$$f(y) = AMc \left(\frac{p_{2\pi/2}}{4i\lambda}, \frac{-p_{2\pi/2}}{2ik}, y \right) + BMs \left(\frac{p_{2\pi/2}}{4i\lambda}, \frac{-p_{2\pi/2}}{2ik}, y \right)$$

and this is just the well known Mathieu equation, whose solution is given in terms of Mathieu functions [11], Mc and Ms :

$$0 = f'' + \frac{d^2f}{dx^2} + \frac{(p\pi)^2}{4} [k - k \cos(2y)] f$$

We now apply the trigonometric relation $\sin(p\pi x) = \cos(\frac{\pi}{2} - p\pi x)$ and make the change of variable $y = \frac{x}{2} - p\frac{\pi}{2}x$. The above equation then becomes:

$$0 = f'' + \frac{d^2f}{dx^2} + \frac{1}{4} \left[k - k \sin(p\pi x) \right] f$$

Another interesting case of a radially oscillatory advection velocity profile, $uV(x) = k \sin(p\pi x)$. The transverse advection diffusion equation becomes:

$$u((\sqrt{u} + \frac{2\sqrt{u}}{q})(\frac{du}{dx})^2) = 0.$$

Note that the original boundary conditions $f(0) = f(L) = 0$ now become $u(\frac{du}{dx}) = 0$

where A and B are integration constants.

$$u(t) = {}^1F_1 \left[\frac{1}{4} \left(1 - \sqrt{\frac{4a}{i}} t \right) \right] A + {}^1F_1 \left[\frac{1}{4} \left(3 - \sqrt{\frac{4a}{i}} t \right) \right] B \sqrt{t}$$

The solution to the preceding equation can be readily obtained in terms of confluent hypergeometric functions, ${}_1F_1$ (see Ref. [11]):

$$0 = u \left[\frac{1}{2} - \sqrt{\frac{4a}{i}} \frac{du}{dt} + \frac{1}{4} \left(\frac{4a}{i} + \frac{1}{4} \right) \frac{d^2u}{dt^2} \right] - \sqrt{\frac{4a}{i}} t$$

and again changing the variable to $t = y^2$. After some manipulation we obtain:

It is perhaps surprising that a continuous transition in the spectrum from the case $\nu = 0$

is obtained in this manner.

The results obtained with the code are in complete agreement with the analytic solution given earlier. Applying Newton's method to the analytical solution has allowed us to determine the eigenvalues for values of the diffusivity as low as $\nu = 10^{-8}$ ($R = 10^9$). This is because in this method we do not have to deal with accuracy problems arising from the real line (i.e., to the continuous spectrum for the purely advective equation). 2) The density of the eigenvalues increases as $R \rightarrow \infty$. 3) The three branches of the spectrum are almost entirely individual eigenvalues will move about in the complex plane. It is essential to note that the spectral distribution does not continuously tend to a subset of the real line (i.e., to the continuous spectrum for the purely advective equation).

We note that the parameter of relevance is the Reynolds (or Feclet, as noted in the introduction) number, $R = \frac{L^2 \nu}{\kappa}$. Note that since $L_x = 1$ in this section, the length used is L_y . It is merely convention, which length is employed in the definition. Furthermore, the eigenvalue spectrum found has the following properties: 1) It is discrete and has a Y shape which is independent of the value of R . This means that no matter how small the shape is, it is non-vanishing, the spectral distribution has a Y shape about it is independent physically which parameter (ν or L_y) is fixed as long as the other varies. The eigenvalue spectrum found has the following properties: 1) It is discrete and has a Y shape which is independent of the value of R . This means that no matter how small the shape is, it is non-vanishing, the spectral distribution has a Y shape about it is independent physically which parameter (ν or L_y) is fixed as long as the other varies. The eigenvalue spectrum found has the following properties: 1) It is discrete and has a Y shape which is independent of the value of R . This means that no matter how small the shape is, it is non-vanishing, the spectral distribution has a Y shape about it is independent physically which parameter (ν or L_y) is fixed as long as the other varies.

We now present the results obtained with the code. Where possible, comparison with analytical solutions is carried out; in all cases excellent agreement is obtained. We first consider profiles of the form $V = kx$, where, k has been set to 10.

In principle, for more complex problems, a judicious combination of numerical and WKB-type asymptotic methods will be needed, especially when R gets very large, as it does in physically realistic problems. The code allows the user to specify an initial guess matrix, a smaller number of iterations on which the Newton's method is supposed to converge, increasing the size of the matrix allows for a choice of variable size. The bigger the number of iterations the likelier it is that all the eigenvalues will be found. Also, increasing the size of the matrix allows for a choice of variable size. That is, good initial guesses will lead to a faster convergence, hence saving computing time in iterations that take too long to converge, if at all, for the bad guesses.

That is, sometimes a better practice than shooting from one boundary. This of the solution and its derivative at an interior point which is judiciously chosen. This method can also be varied by starting from both boundaries and imposing "continuity" condition until a convergence criterion such as $|f(1, \lambda)| < \epsilon$, where ϵ is the desired precision, is satisfied.

$$\lambda^{j+1} \text{ is now the new trial value, and a new solution, } f(1, \lambda^{j+1}) \text{ can be calculated. The formula is given by}$$

$$\lambda^{j+1} = \lambda^j - \frac{\frac{\partial f}{\partial \lambda}|_{\lambda=\lambda^j}}{f(1, \lambda)}$$

equation $f(1, \lambda) = 0$, can then be used to converge on the eigenvalue. The iteration

We next consider a purely sinusoidal profile, $V(x) = k \sin(n\pi x)$, where n is some integer and k is a constant. Analytical solution is possible, as shown earlier. The agreement between numerical and semi-analytical results is again found to be entirely satisfactory. In this case, degeneracy in the eigenfunctions (ie., different eigenfunctions associated with the same eigenvalue) is to be expected due to symmetry considerations. The domain is geometrically invariant upon a 180° rotation, making this situation similar to the cubic box potential for the Schrödinger equation, where degeneracy is known to occur. An example of the eigenvalues is given in Figure 5.

In the case of a parabolic profile $mV = kx^2$, where k has again been set to 10, the spectrum was found to have the same general properties as the linear case (invariance for the value of the diffusivity and increase in the density of the eigenvalues as $R \rightarrow \infty$), except that now the Y shape is no longer symmetric. The left arm now makes a 45° degree angle with the horizontal, thus implying that eigenvalues in this region have symmetric real and imaginary parts. Figure 4 illustrates this for two different values of the diffusivity. Comparisons with semi-analytical results again yields excellent agreement, as can be seen in Figure 5.

In the case of a parabolic profile $mV = kx^2$, where k has again been set to 10, the spectrum was found to have the same general properties as the linear case (invariance for the value of the diffusivity and increase in the density of the eigenvalues as $R \rightarrow \infty$), except that now the Y shape is no longer symmetric. The left arm now makes a 45° degree angle with the horizontal, thus implying that eigenvalues in this region have symmetric real and imaginary parts. Figure 4 illustrates this for two different values of the diffusivity. Comparisons with semi-analytical results again yields excellent agreement, as can be seen in Figure 5.

It should be stated that for large Reynolds numbers, it becomes difficult to find the eigenvalues with the computer code. This is due to two reasons: 1) As the value of R increases, the variations in the solution, $f(x)$ increase too. Hence, the space step has to be made increasingly smaller to cope with this, until it becomes computationally impractical to solve the equations. 2) The density of the eigenvalues increases as R increases. At a certain point they will be so close to each other that Newton's method has difficulty in converging. A more robust technique like interval-halving can then be used, with some care in the choice of the interval, in judicious combination with an analytic asymptotic convergence. A more robust technique like interval-halving can then be used, with some care in the choice of the interval, in judicious combination with an analytic asymptotic convergence. It is notable that Newton's method has difficulty in converging. A more robust technique like interval-halving can then be used, with some care in the choice of the interval, in judicious combination with an analytic asymptotic convergence. A more robust technique like interval-halving can then be used, with some care in the choice of the interval, in judicious combination with an analytic asymptotic convergence.

This discussion is not a new result and has been addressed in papers by Lortz [12] and Dewar and Davies [13], in connection with the corresponding phenomena in ideal MHD. The mathematical explanation for this “paradox” (ie., the ideal and dissipative spectra have different morphology in the limit as the diffusivity goes to zero) is due to the fact that diffusion is a *parabolic singularity*. The examples given earlier elucidate this advective (ie., hyperbolic) equation. The examples given earlier elucidate this advective (ie., hyperbolic) equation. The examples given earlier elucidate this advective (ie., hyperbolic) equation. The examples given earlier elucidate this advective (ie., hyperbolic) equation. The examples given earlier elucidate this advective (ie., hyperbolic) equation.

Main results may be summarised as follows: 1) The spectrum has as many branches $V_{01} \neq V_{02}$ or make distances of the jets' centres to the boundary walls different. In Figure $x_{02} = 0.65$). This degeneracy translates itself in the eigenvalue spectrum as overlapping and $x_{01} = 0.35$. In this situation there are two obvious ways to remove the degeneracy: either make arms. Jets are equally spaced from the boundaries of the domain (say, for instance, $x_{01} = 0.35$ and $x_{02} = 0.65$). Geometric degeneracy occurs if the domain is invariant under rotation/reflection. For example, in the case of a double jet profile, there will be degeneracy if $V_{01} = V_{02}$ and x_{01} are considered the double jet case, the spectrum will have a three arm structure. 2) as the number of regions into which the domain is divided. Thus, for instance, if we are considering the double jet profile, the spectrum is divided into three regions.

Good agreement was obtained between numerical and analytic eigenvalues. Matching solutions from the different regions and using the boundary conditions. Very equation is trivial in each sub-region of the domain. Eigenvalues can thus be obtained by that the profile is either zero or constant, solution to the governing advection-diffusion given 26 the total width of a jet (supposed same for both jets). Elsewhere $V(x) = 0$. Given where V_{01} and V_{02} are the constant heights of the jets, x_{01} and x_{02} their centres and

$$V(x) = \begin{cases} V_{02}, & x_{02} - \delta < x < x_{02} + \delta \\ V_{01}, & x_{01} - \delta < x < x_{01} + \delta \end{cases}$$

effect of a profile composed of two of these jets, that is: produce similar changes in advective (ie., electron inertial) terms. We have studied the pressure gradient. In the case of electron physics, current gradients and dynamics driven by both turbulent Reynolds and Lorentz forces/stresses and corrugations in the ion sufficient to validate all the following conclusions). Physically, this kind of profile can be of the domain, where it assumes a high value (typically, a Reynolds number $R = 10^4$ is By a "jet" profile we mean a velocity field that is zero everywhere except in a small region

reciprocal case of perturbing the sinusoidal potential with a linear one. 7 and 8 illustrate this continuous transition. The same reasoning obviously applies in the regularity operator $L = L_0 + \epsilon L_1$ as the perturbation L_1 is switched on. Figures discrete) of an unperturbed operator L_0 changes continuously into the point spectrum of a can be used to explain the transition. According to this theorem, a point spectrum (ie. As seen earlier, this operator has a point spectrum. A standard theorem due to Kato [14]

$$L_0 = i\nu \frac{d^2}{dx^2} + k_1 x$$

small perturbation to the unperturbed operator. If k_2 is made very small, then we can think of the sinusoidal component in Eq.(18) as a One question is how the transition from the linear profile to that given in Eq.(18) occurs.

$$(18) \quad V(x) = k_1 x + k_2 \sin(n\pi x)$$

profiles where this undesired effect has been eliminated, of the form: The introduction of a linear contribution to the profile, however small, immediately destroys this symmetry, thus removing degeneracy. It is then more interesting to analyse profiles where this undesired effect has been eliminated, of the form:

example can be seen in Figure 6.

CADENCE was developed as the precursor of a new fully 3-D turbulence code for realistic tokamak geometries, which is why the second transverse direction is included in the above

very efficiently. Eq.(19) and re-arranging to produce a tridiagonal matrix equation in f that can be solved to be given. The function f is evolved in time by forming a finite difference equation from boundary values $f(x=0, y, z, t), f(x=1, y, z, t)$ and the initial condition, $f(x, y, z, t=0)$ $f(x, y, z, t) = f(x, y + 2\pi, z, t)$ and $f(x, y, z, t) = f(x, y, z + 2\pi, t)$. We assume the radial coordinate $0 \leq x \leq 1, 0 \leq y, z \leq 2\pi$, with f periodic in y and z such that $f(x, y, z, t) = f(x, y + 2\pi, z, t)$ and $f(x, y, z, t) = f(x, y, z + 2\pi, t)$. Thus, CADENCE solves for $f = f(x, y, z, t)$ in the domain (using a nondimensional

general) complex-valued functions of x, y and z . Here, a second transverse advection term is present, and there are also "radial" advection terms, source (S) and growth rate (g) terms. The coefficients of all the terms are (u_x), (in

$$S + fu_y + \left(\frac{x\partial}{f\partial} D \right) \frac{x\partial f}{\partial} = (fu_x) \frac{x\partial}{\partial} + \frac{z\partial}{f\partial} u_z \frac{y\partial}{\partial} + \frac{u_y\partial}{f\partial} + \frac{\partial}{f\partial} g \quad (19)$$

The general form of the equation solved by CADENCE is a variation on Eq.(1):

We next describe the CADENCE code which treats advection-diffusion equations like Eq.(1) using parallel processing clusters by solving the appropriate initial-boundary problem. For simplicity, we only consider the case of purely radial diffusion, denoting the diffusivity in this section by D . The code solves problems in three spatial dimensions. As before, the x direction corresponds to the "radial" direction, whilst the y, z directions correspond to "poloidal" and "toroidal" directions in a tokamak [5].

IV. Solutions of the initial value problem for the advection-diffusion equation: the evolutionary approach

The confinement of the eigenfunctions is an interesting result and should be of importance in the limiting of radial correlations and propagation effects associated with the turbulence. Hence, it may alter the turbulent transport. Results are obviously generalizable for an arbitrary number of jets. It should be noted that this type of "ge-het-to-isation" of transported scalars by advection-diffusion equations was already foreseen in an astrophysical context in an earlier investigation by Parker and one of the authors [8].

Different regions of the domain are isolated from each other, implying that eigenfunctions will approach zero values near the jets, as can be seen in Figure 10. For high enough Reynolds numbers ($R = 10^5$ is already sufficient) eigenfunctions will only exist in one of the three regions in which the jets divide the domain. We have thus found that this kind of velocity profile confines the eigenfunctions in the regions between the jets. Each branch of the eigenfunction starts for one of these regions.

⁹ we show a situation where degeneracy has been removed by displacing one of the jets. 3)

Figure 16 demonstrates graphically the evolution of the $D = 0$ case described earlier, as calculated by CADENCE. The cascade of energy into higher and higher wave numbers is immediately apparent. The initial function f has a $\sin 2y$ variation, and this is preserved at all x values at all times, but the number of waves in the x direction rises steadily.

Fast Fourier Transform algorithms do not “interact” in this linear model). All Fourier transforms are carried out using the formula, and then into a tridiagonal matrix equation for each k value (ie. the different F_k ($S_k = 0$ except for $k = 0$ in our case)). This is straightforward to translate into a difference

$$\begin{aligned} \frac{\partial F_k}{\partial t} &= D \frac{\partial^2 F_k}{\partial x^2} - ik u_y F_k + S_k & (22) \\ f(x, y, t) &= \sum_{k=-\infty}^{\infty} F_k(x, t) e^{iky} & (21) \end{aligned}$$

The equation may be solved by expanding $f(x, y, t)$ in a Fourier series with respect to y and then applying the differential equation to each component:

If R is high, advection dominates, whereas, for R low, diffusion dominates. Here, since $L_x = 1$, u_0/D_0 is the Reynolds/Peclet number R , which can take any value.

$$\begin{aligned} f(x = 1, y, t) &= 0 \\ f(x = 0, y, t) &= 0 \\ f(x, y, t = 0) &= x^2(1 - x^2) \sin 2y \end{aligned} \quad (20)$$

For the purposes of this paper, we will use a cut-down version of Eq. 19 to demonstrate how CADENCE has been used to provide extra insight into the results from the eigenvalue code considered earlier. The two approaches validate each other's findings, but also bring out complementary properties in the advection-diffusion equation. Here, we restrict ourselves to a single transverse direction, exclude radial advection and growth rate terms, and consider typical initial values and boundary conditions given by

course of the calculation the function values at these points are passed from one processor to another to ensure continuity in the solution. This is achieved by “overlap” so that they have two common elements, and during the adjacent processors’ time-step. Figure 15 shows how the distribution of x elements is arranged; after each time-step, passing appropriate values of f to its “neighbouring” processors in its own sub-domain, and each processor solves the partial differential equation one for each of the n_p processors, and each processor solves the partial differential equation x domain is split into n_p equal sub-domains (these are usually or layers in the x direction); provides a convenient method of parallelising the code onto a number of processors. The much longer in the radial direction than in the poloidal and toroidal directions, and this equation. A property of tokamak plasmas is that the timescale for transport effects is

The key conclusions of our studies are summarised as follows: in the absence of diffusion, purely advecting systems, although conserving energy, can lead to an "ultra violent" catastrophe. This manifests itself in a "direct cascade" where the shared flows "phase mix" structures transverse to flows and the energy is transported in radial wave number space to arbitrarily high wave numbers. Spatially the transported property acquires radial "fine structure" or "corrugations" [5, 6] seen in much more general nonlinear simulations. Purely diffusive systems, on the other hand, imply a simple damping by the energy directly proportional to the diffusivity. This damping can be very weak when the damping by even small diffusivity in the presence of shear and advection transverse to the smooth. What we have sought to demonstrate is that the damping rate is greatly enhanced by the exact and the numerical solutions that the damping rate is greatly enhanced by the shear and the damping by even small diffusivity in the presence of shear and advection transverse to the damping by the shear and the damping rate is relatively small due to the latter's phase mixing capacity. Thus, qualitatively speaking, both by the shear and the damping rate is greatly enhanced (also confirmed by the direct simulation of diffusion). It is easy to see from dimensional arguments alone that the damping by the shear and the damping rate is greatly increased due to the shear and advection transverse to the damping by the shear and the damping rate is relatively small due to the latter's phase mixing capacity. Thus, qualitatively speaking, both by the shear and the damping rate is greatly enhanced (also confirmed by the direct simulation of diffusion).

In this paper, we have considered a paradigmatic analysis of one of the simplest nonself-adjoint equations, namely, the linear advection-diffusion equation. In important cases, the equation is exactly soluble in terms of well-known functions. It has special cases, the equation is approximately soluble in terms of well-known functions. It has been found possible to treat its spectral properties relatively generally using the Green's function approach (alternatively called the "resolvent" method). These analytic techniques are supplemented by an eigenvalue approach and an evolutionary initial value approach using standard numerical algorithms. These methods apply in course to far more complicated and realistic systems of parabolic differential equations encountered in fluid mechanics and plasma physics.

V. Discussion and conclusions

In Section III above, it was pointed out that the eigenvalue code described there has difficulty in finding eigenvalues for small values of D . In contrast, the eigenvalue code used in this way CADENCE has been used successfully to verify the eigenvalues and the spectra for all of the more complicated cases described earlier. For instance, Figure 19 shows the final solution of the double-jet run shown in Figure 12, as calculated by CADENCE. The initial function was a delta function at $x = 0.05$, varying as y in the y -direction. As expected, the initial function spreads out in x , but is confined by the left hand jet. The slope of the $\log E(t)$ curve tends towards a value of 0.0824, in agreement with the calculation by the eigenvalue code.

Compare this result with Figure 17, which introduces a small ($D = 10^{-4}$) diffusivity into an otherwise identical problem. The diffusion, though apparently insignificant, still wins out because of its strong decay of high- k_x waves as predicted earlier. In fact the combination of advection as well as diffusion causes a much faster reduction in the energy than is out because of its strong decay of high- k_x waves as predicted earlier. In fact the combination of advection as well as diffusion causes a much faster reduction in the energy for $E(t) = \int \int f^2 dx dy$ of the system, as shown in Figure 18, which compares $E(t)$ for advection-only, diffusion-only and advection + diffusion cases.

radiation damping of a charged particle in classical electromagnetic theory. These are of “continuum” damping by shear Alfvén waves, a concept intimately related to the advection-diffusion effects have not yet been fully explored. Closely related is the notion by highly sheared advective effects from the streaming terms. These “velocity space” from simple collisional (i.e., diffusive in velocity space) decay, by being strongly enhanced collisionality”. The effective relaxation rates could conceivably be higher than expected in linear limits, the purely collisionless spectral properties of the Vlasov dispersion equation of plasma physics. The Fokker-Plank-Landau Coulomb collision/Fokker-Plank collisions are included in the Vlasov equation, one obtains the Boltzmann/Fokker-Plank operator is hyperbolic and plays the role of advection in phase space. When binary operator” is hyperbolic and plays the role of advection in which the “streaming

It is worth noting that the collisionless Vlasov equation is one in which the tokamaks [16].

and radial propagation of heat and density pulses in transient experiments conducted on to be intimately linked to the formation and dynamics of “internal transport barriers” to the interplay of radial advection and diffusion is thought plasma transport processes. The interplay of radial advection and important role in applicable. This type of advection-diffusion equation also has a very important role in operator, and variational methods of determining spectra and eigenfunctions become interacting with radial diffusion. In this case, the problems are reducible to Hermitian nature of the evolution. Another well-known application [15] is to purely radial advection of the system (with respect to the “slow” time, of course) and obtain insight into the themselves, it is possible to define in a meaningful fashion, the “instantaneous” spectra the advection terms change relatively slowly in time compared to the shearing rates geophysical/aerophysical situations [5]. Indeed, it is also demonstrated that regions of parabolic equations involving

The methods described here can also be applied to systems of parabolic equations involving its fully nonlinear forms) is ubiquitous in the consideration of such transport properties. transport temperature and magnetic flux, and the advection-diffusion equation (albeit in currents, which are usually flows of the electron fluid. Electron flows can (and do) created by the turbulence itself. Of course, the considerations extend to effects produced geophysical/aerophysical situations (e.g. as in [8]) where strong jet-like flows can be “ghettos” in the transport properties. This could be effective in both plasmas and in We have also demonstrated that regions of highly sheared flows can “confine” or create

our results.

flows also provide an important route to direct cascades of energy is clearly illustrated by “stabilization” of turbulence studied in several recent works in tokamak physics. That such enhancement damping rates may at least be partially responsible for the so-called “shear flows elsewhere that the limits are nonuniform. The capacity of sheared advective flows to are necessarily singular perturbations and it has long been known in fluid mechanics and necessary to those of the latter. Parabolic effects caused by irreversible diffusion of the fact that the properties of parabolic systems “close” to hyperbolic ones do not the limit as the diffusivity tends to zero. This “paradox” is merely the consequence systems are not approached uniformly by those of the advection-diffusion system in is also associated with the fact that the spectra of the purely advective (conservative)

- [11] M. Abramowitz and I.A. Stegun, *Handbook of mathematical functions*, Dover, (1972).
- (1969).
- [10] E.C. Titchmarsh, *Eigenfunction Expansions*, I, Oxford University Press, Oxford, UK,
- Holland, Amsterdam, (1967).
- [9] N.G. Van Kampen and B.U. Felderhof, *Theoretical Methods in Plasma Physics*, North
- Evanston, IL, USA, (1999).
- [8] E.N. Parker and A. Thyagaraja, *Solar Physics*, **189**, 45, (1999).
- [7] A. Thyagaraja, *Journal of Plasma Physics*, **59**, 367, (1998).
- (2001).
- [6] C.N. Laschmore-Davies, D.R. McCarthy and A. Thyagaraja, *Phys. Plasmas*, **8**, 5121
- (2001).
- [5] A. Thyagaraja, *Plasma Phys. Control. Fusion*, **42**, B255, (2000).
- [4] P.N. Guzdar, R.G. Kleva and Liu Chen, *Phys. Plasmas*, **8**, 459 (2001).
- [3] A.I. Smolyakov, P.H. Diamond and V.I. Shevchenko, *Phys. Plasmas*, **7**, 1349 (2000).
- [2] Z. Lin, et al., *Phys. Rev. Lett.*, **83**, 3645 (1999).
- [1] K.H. Burrell, *Science*, **281**, 1816 (1998).

References

The authors would like to thank Terry Martin for his help in the configuration of the Aethelwulf parallel cluster. N.L. acknowledges with thanks, Fundacao para a Ciencia e a Tecnologia, Ministerio da Ciencia e do Ensino Superior, Portugal for their support. This research was supported by EURATOM and the Dept. of Trade and Industry, UK.

Acknowledgements

Since the advection-diffusion equation itself is a very generic transport equation appearing naturally in transport problems in many different fields, our methods and results can be expected to have a much wider domain of applicability than the original motivation provided by the shear flow paradigm in current tokamak research. Finally, by separating the problem of the genesis of sheared advective flows from that of studying their consequences in a simple but widely applicable setting, valuable insight into the nature of transport and the effects of sheared flows has been attained.

best illustrated by invoking a small but finite dissipation in the system which "resolves" the continuum, but nevertheless, the dissipation rate itself becomes independent of the appropriate analogue of the Reynolds number.

- [12] D.Lortz and G.O.Spies, Phys. Letters **101A**, 7, (1984).
- [13] R.L.Dewar and B.Davies, J. Plasma Physics, **32**, 3, (1984).
- [14] T.Kato, *Perturbation theory for linear operators*, Springer, (1976).
- [15] A.Thyagaraja and F.A.Haas, Physica Scripta, **41**, 693, (1990).
- [16] P.Marticca *et al.*, Phys. Rev. Lett., **85**, 4534, (2000).

Figure 2: Same as previous graph but $\nu = 0.01$. Squares denote points calculated numerically, crosses denote semi-analytical results. Notice the convergence of the branches in the same point as before.

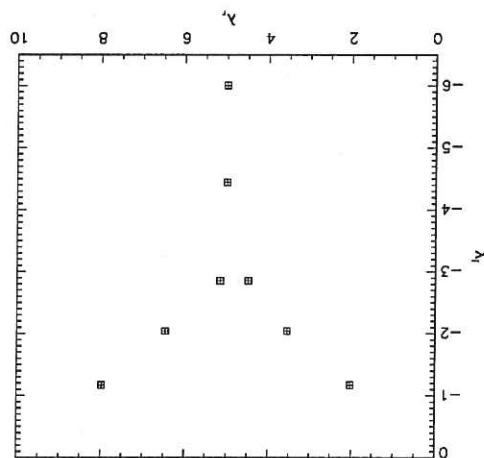


Figure 1: Eigenvalue spectrum for velocity profile $V(x) = 10x$ and $\nu = 0.001$.

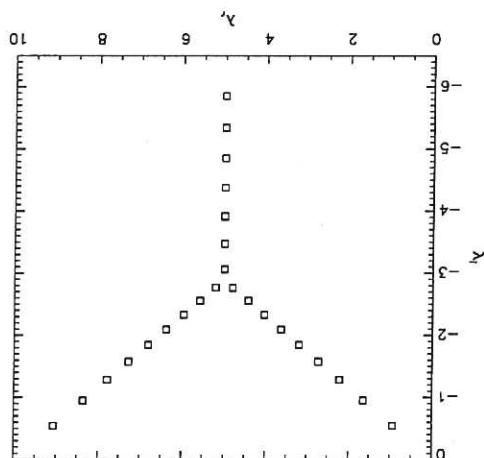


Figure 4: Eigenvalue spectrum for the parabolic velocity profile $V(x) = 10x^2$ and $\nu = 0.001$ (squares) and $\nu = 0.01$ (crosses). The overall structure is also independent of the value of the diffusivity.

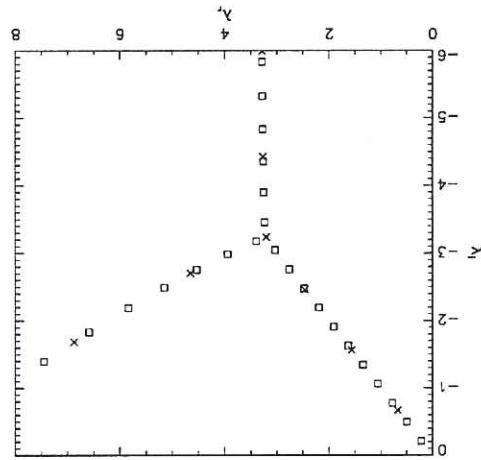


Figure 3: Semi-analytical solutions for same linear profile. Squares denote solutions with $R = 10^6$, crosses denote $R = 10^9$ results. Both spectra are incomplete; again notice the exact overlap of the overall structures, showing independence of the value of ν ; also, an increase in the eigenvalue density is clear.

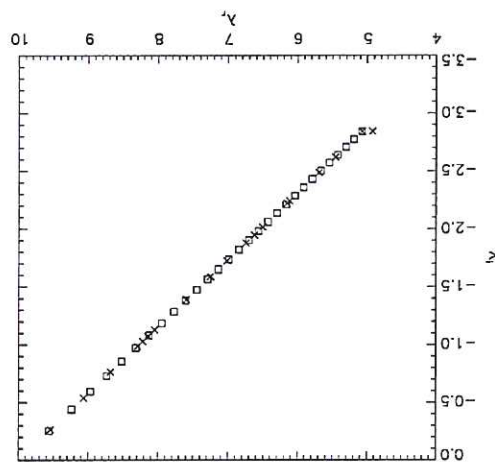


Figure 6: Eigenvalue spectrum for sinusoidal profile $V(x) = 10 \sin(8\pi x)$. More than one eigenfunction corresponds to the same eigenvalue.

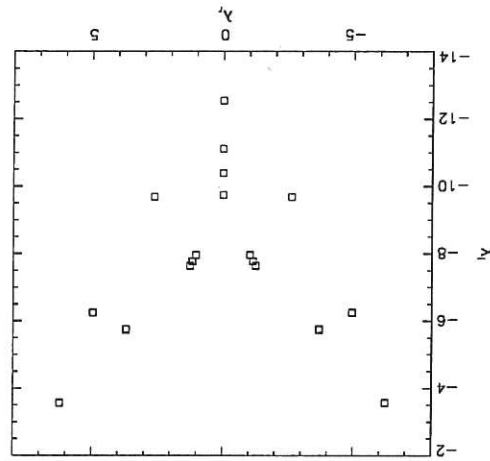


Figure 5: Numerically obtained eigenvalues (squares) versus some semi-analytic results (crosses): very good agreement can be observed.

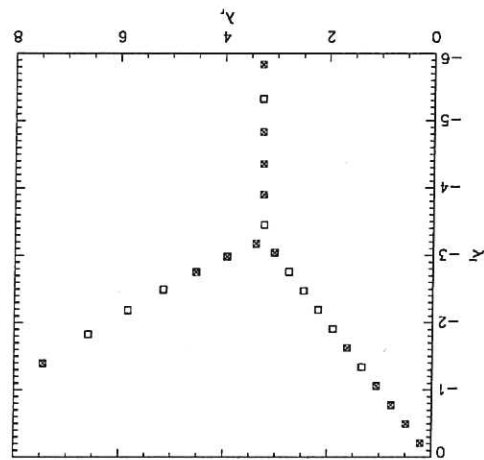


Figure 8: Compare with Fig. 7. As the sinusoidal contribution is increased so that $k_2 = 0.1$, the Y shape gets more deformed.

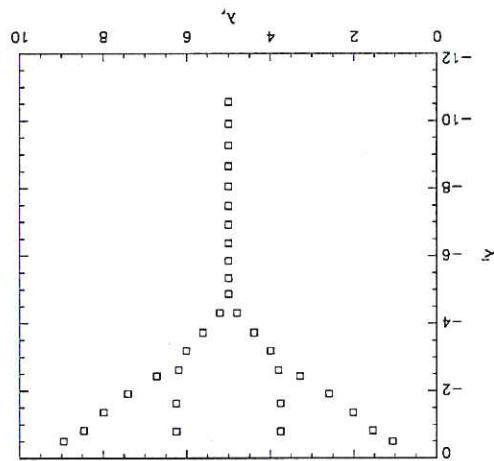


Figure 7: Spectrum for $V(x) = 10x + 0.01 \sin(8\pi x)$. Note how the Y shape from the purely linear profile is subtly deformed

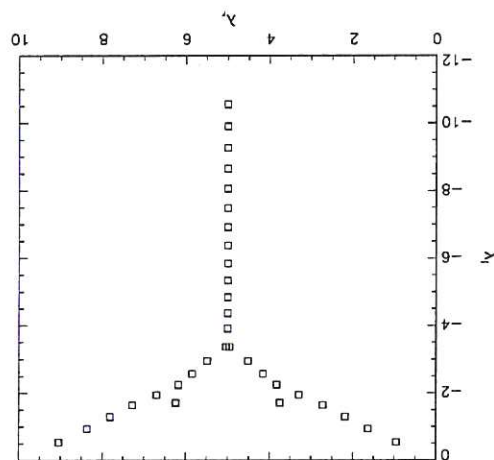


Figure 10: Lowest order mode for a $R = 10^4$ double jet velocity profile. The jets are placed at $x_{01} = 0.35, x_{02} = 0.65$, with width $\delta = 0.01$. Eigenfunction has nearly zero values in the highly sheared vicinity of the jets, meaning that the three regions are isolated.

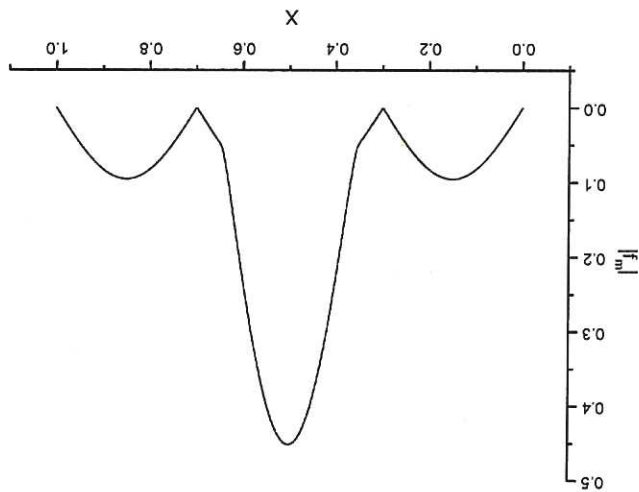


Figure 9: Spectrum for double jet profile: $V_{01} = V_{02} = 500; x_{01} = 0.35; x_{02} = 0.80;$ $\delta = 0.005$. Three independent branches can be seen: degeneracy has been removed by breaking symmetry through displacement of one of the jets.

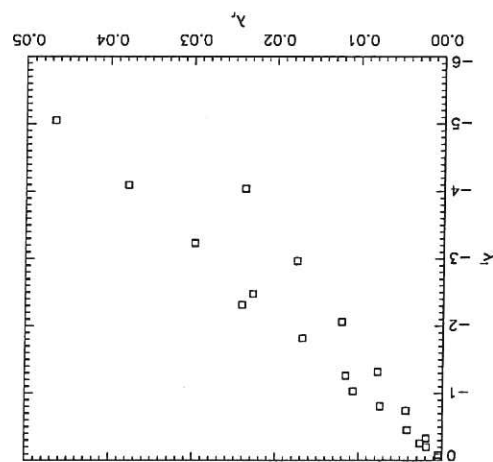


Figure 12: Lowest eigenfunction of the left arm for a double jet profile with $V_{01} = -V_{02} = 500$. Complete confinement of the eigenfunction is observed.

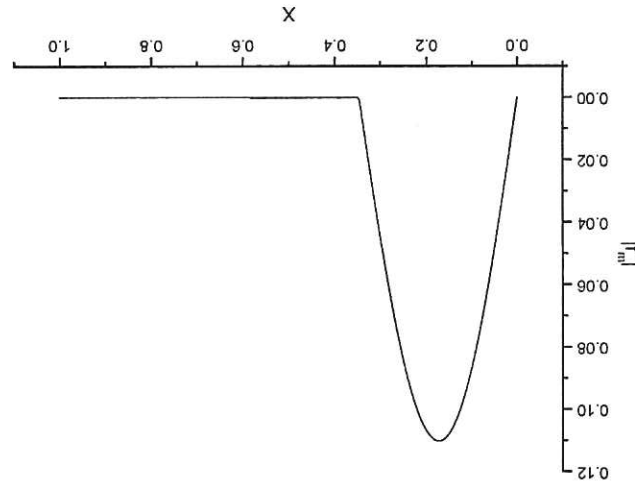


Figure 11: Eigenvalues for two different double jets profile. Squares denote the results for $V_{01} = -V_{02} = 100$, while crosses denote the results for $V_{01} = -V_{02} = 500$. It can be seen how increasing the height of the jets makes $\lambda_i \rightarrow 0$.

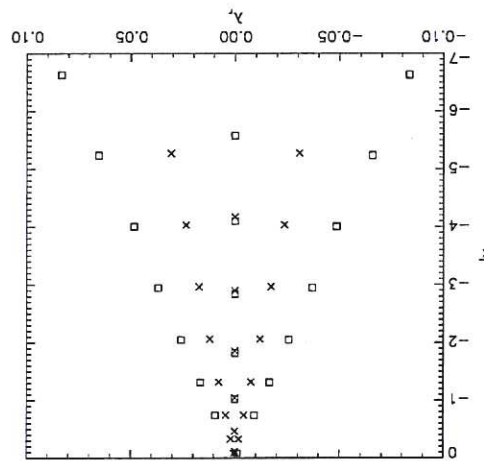


Figure 14: Same as above but for the central arm.

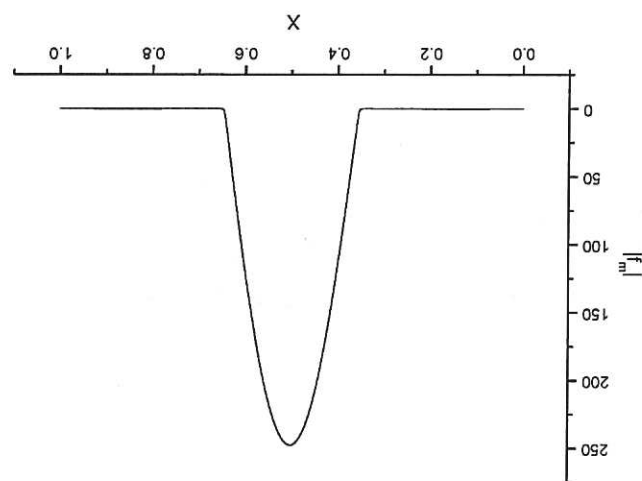


Figure 13: Same as above for the right arm.

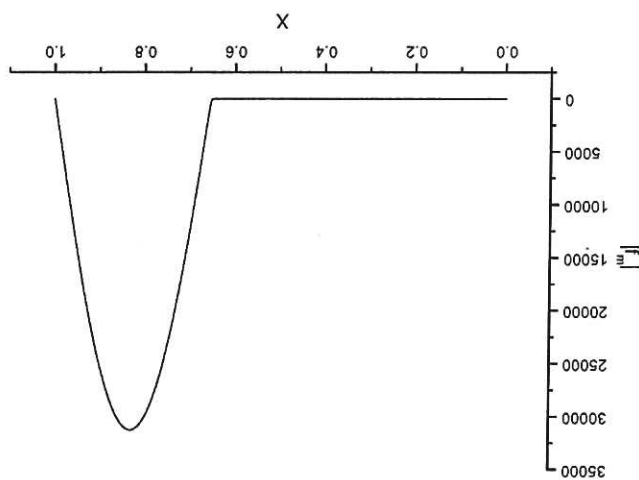


Figure 16: CADENCE calculation of the evolution of a function $f(x, y)$ with transverse fixed y . The increase in radial wave number k_x is immediately apparent. The middle plot is f at $t = 30$ s, and the right plot shows the evolution in time of f at a advective $u_y(x) = -x$, in the absence of diffusion. The left plot is the initial state of f , the middle plot is f at $t = 30$ s, and the right plot shows the evolution in time of f at a

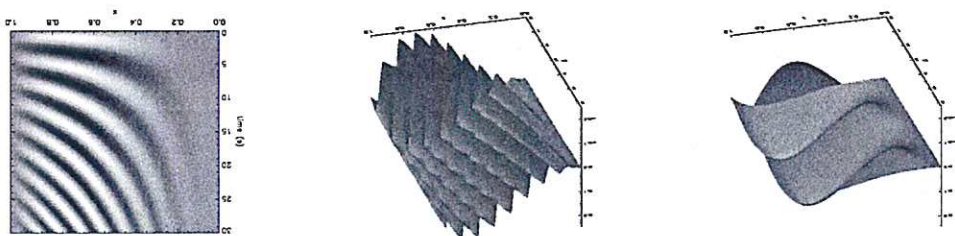


Figure 15: Distribution of x elements between three processors. During each solution cycle the values of f at the elements near the internal boundaries between adjacent processors are passed in the direction indicated. Processor $(k + 1)$ evolves f_1 via the solution of the matrix equation and passes the value into f_n on processor k , and processor $(k - 1)$ evolves f_{n-1} and passes the value into f_0 on processor k .

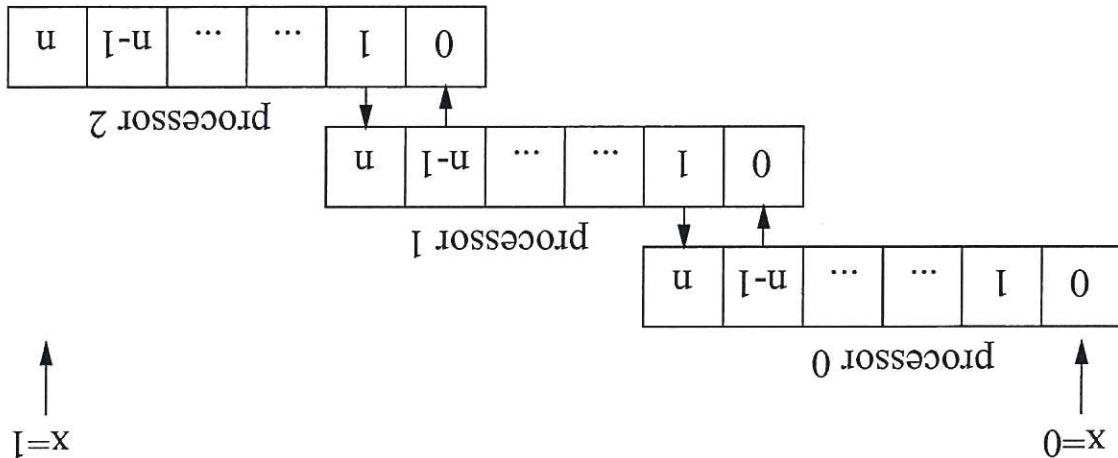


Figure 17: CADENCE calculation of the evolution of the same initial function $f(x, y)$ as in Figure 16 but with the addition of a small amount of diffusivity, $D = 10^{-4}$. The Left hand plot is the state of f after $t = 30$ s, and the right hand plot shows the evolution in time of f at a fixed y . The preferential decay of the high k_x waves is clear.

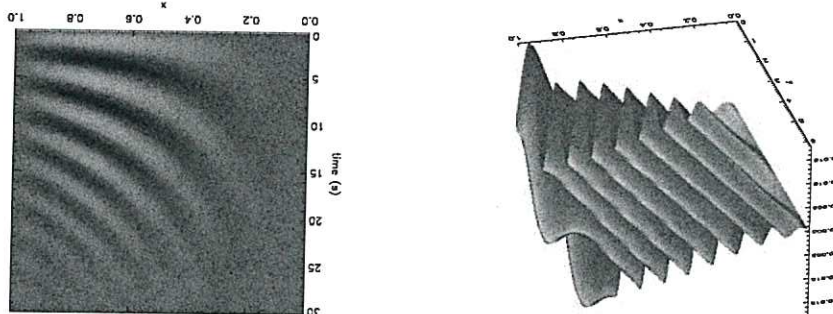


Figure 18: CADENCE calculation showing how the rate of change of total energy $E(t) \equiv \int f^2 dx dy$ varies for three different cases. (1) advection $u_y = -x$, no diffusion (solid curve); (2) diffusion $D = 10^{-2}$, no advection (dotted curve); (3) both advection $u_y = -x$ and diffusion $D = 10^{-2}$ (dashed curve).

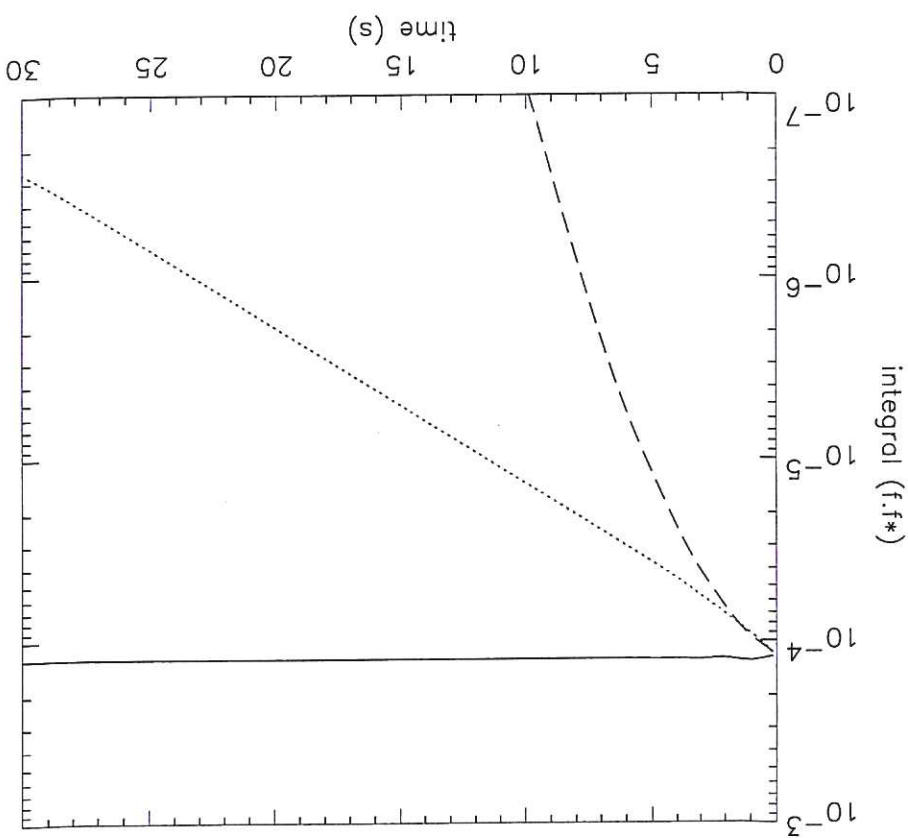


Figure 19: CADENCE calculation of the double jet case of Figure 12, showing the confinement of the function by the left hand jet at $x = 0.35$. The amplitude plot on the left shows the final eigenfunction, and is the same as that calculated by the eigenvalue code. The integral plot on the right shows the decay of $E(t)$ with time, and the final gradient gives the eigenvalue as 0.0824, again in agreement with the eigenvalue code.

